Polar-optic phonons and high-field electron transport in cylindrical GaAs/AlAs quantum wires

X. F. Wang
Shanghai Institute of Metallurgy, Chinese Academy of Sciences, 865 Changning Road, Shanghai 200050, China

X. L. Lei
China Center of Advanced Science and Technology (World Laboratory), P.O. Box 8730, Beijing 100080, China and Shanghai Institute of Metallurgy, Chinese Academy of Sciences, 865 Changning Road, Shanghai 200050, China

(Received 18 June 1993)

Linear and nonlinear electron transport in GaAs/AlAs cylindrical quantum wires is investigated with the help of the balance-equation transport theory. Confined phonons, surface phonons, and their Fröhlich couplings with electrons in these quasi-one-dimensional electron-phonon systems are described using the dielectric continuum, hydrodynamic continuum, and Huang-Zhu optic-phonon models, respectively. Both intrasubband and intersubband transitions of up to 21 electron subbands are taken into account in the numerical calculation. The comparison of the results from these three models with those obtained by using bulk phonon approximation shows that the bulk phonon approximation is accurate enough to describe the Fröhlich interaction when calculating the linear and nonlinear electron transport even in ultrafine GaAs/AlAs quantum wires.

I. INTRODUCTION

Since the observation of confined optic phonons in GaAs/AlAs superlattices,[1] phonon modes in semiconductor microstructures have been the central focus of many experimental[1-3] and theoretical[4-15] investigations. Microscopic[5,6] and macroscopic[7-17] models have been developed to describe the longitudinal optic (LO) phonons and estimate the electron-phonon interactions in various confined systems. To avoid the labored numerical computation required in the calculation of electron transport in low-dimensional electron-phonon systems using microscopic phonon models, people have been attempting to find a proper analytical description of optic-phonon confinement for the past several years. Three kinds of analytical models for polar-optic phonons have been widely used in the literature.

The first is known as the dielectric continuum (DC) model, or slab model, in which the optic-phonon modes are determined by the electrostatic boundary condition. The DC model anticipates that there exist two kinds of distinct optic-phonon modes, bulk-like modes (confined phonons), and interface modes (surface phonons) in GaAs/AlAs heterostructures. The bulklike modes have vanishing electrostatic potential and maximum normal optic displacement at the GaAs/AlAs interface.[9,10,16]

The second model, the so called hydrodynamic continuum (HC) model, or guided model, is developed by use of the mechanical boundary condition. In the HC model the bulklike modes are guided modes, which have a node at the boundary for the normal optic displacement and an antinode for the electrostatic potential. Whether or not there exist interface modes is still in dispute.[5,10-12,18]

The third model was developed by Huang and Zhu[6] from a simple microscopic model and will be called the HZ model in this paper. This model suggests that both the normal optic displacement and the electrostatic potential vanish at the GaAs/AlAs interface.

Quantum wires of various geometries have recently been fabricated for studies of phonon and electron properties[19-22] with the help of advanced growth and microfabrication technologies such as molecular-beam epitaxy and selective ion implantation. Surface phonons were observed in cylindrical GaAs quantum wires[19] in Raman-scattering experiments. Electron transport in quantum wires was also studied experimentally and the current oscillation due to electron confinement was discovered.[21] The research of the electronic energy relaxation and transport property in quantum wires has become another focus in the field of low-dimensional semiconductor physics.[4,23,24]

Because of the importance of optic phonons in semiconductor microstructures and the long-standing theoretical controversy[10-18,25-28] regarding the validity of different analytical models, the comparison among electron-phonon scattering rates resulting from different optic-phonon models has become an interesting subject in the literature. Rücker and co-workers[5] calculated the scattering rates in GaAs/AlAs quantum wells using a microscopic description of phonon spectra and DC, HC, and HZ models. They found that results from different models might be completely inconsistent. Rudin and Reinecke[29] compared intrasubband and intersubband scattering rates of electrons in the lowest two subbands of quantum wells, obtained from different phonon models, and suggested that the macroscopic (DC and HC) models are not appropriate for a quantitative evaluation of phonon contribution to the electron relaxation rates. Weber, de Paula, and Ryan[30] calculated the electron scattering rates using the HZ model and found

good agreement with experimental results. Tsuchiya and Ando[15] made a detailed investigation of transport properties in superlattices using the bulk-phonon approximation, an envelope-function approximation, and the DC model to describe optic phonons and found that even the bulk-phonon approximation explains the layer thickness dependence of the electron scattering rate reasonably well. Recently, Nash[14] pointed out that electron-phonon scattering rates in quantum wells are independent of the basis set used to describe the phonon modes as long as this set is orthogonal and complete. He developed[14] a dispersive continuum theory of lattice dynamics for semiconductor heterostructures in which the phonon modes of the three phonon models mentioned above are the normal modes in the limit of infinitesimal dispersion at different circumstances. Ridley and co-workers[27] and Constantinou[28] described the optical-phonon modes in quantum wells with a theory involving the hybridization of LO, TO, and interface polariton (IP) modes lately. In addition, there are many other papers that are devoted to a theoretical discussion of the validity of various phonon models in quantum well [10,18,25,26] or to the calculation of the electron transport properties by employing different phonon models.[29–34]

Recently, optic-phonon models in quantum wires have been studied in the literature. Stroscio and co-workers[16] proposed the confined and surface optic-phonon modes in a rectangular quantum wire within the framework of the DC model and calculated their scattering rates with electrons. They concluded that the surface phonons play a prominent role in contributing the scattering rate when both phonons and electrons are confined in extremely narrow quantum wires. Knipp and Reinecke[17] criticized that the results deduced in Ref. 16 did not properly include the DC boundary condition. They derived analytically the interface modes for wires of elliptical cross sections by incorporating the DC boundary condition, and pointed out that the interface modes for wires of more general cross section cannot be obtained analytically in the DC model. Enderlein and Selbmann[35] studied the optic-phonon modes of circular quantum wires by means of the generalized Born-Huang equation with the Hermiticity condition for the dynamical operator and deduced the corresponding Fröhlich interaction in GaAs quantum wires which is similar to that obtained from the DC model. Constantinou and Ridley[36] have detailed the optic-phonon modes in cylindrical $GaAs/Al_xGa_{1-x}As$ quantum wires using the HC model. The HZ model has recently also been extended to rectangular quantum wires by Zhu.[6] The continuum phonon model of optical hybrids was applied to a cylindrical wire by Constantinou.[28] Other authors also contributed to the exploration of optic-phonon modes or electron-phonon scattering rates in quantum wires.[24] Nevertheless, phonon modes of the HZ model have not yet been studied in cylindrical quantum wires. Furthermore, there has so far been no paper devoted to the comparison of electron transport in quantum wires using different phonon models, and the phonon confinement effects on nonlinear electron transport have not been shown in the literature.

The purpose of the present work is to investigate the linear and nonlinear electron transport in GaAs/AlAs cylindrical quantum wires with different lateral confinements by employing the three different (DC, HC, and HZ) LO phonon models. The calculations are based on the balance-equation transport theory of Lei and Ting.[23,37] Contributions of both confined and surface optic phonons, if any, are considered through the Fröhlich interaction. Other kinds of electron-phonon interaction mechanisms (deformation potential scattering with longitudinal optic and acoustic phonons and piezoelectric interaction with acoustic phonon) are also included, but treated using the bulk phonon approximation (BK). To study the high electric field properties, intrasubband and intersubband electron transitions of up to 21 subbands are taken into account. The paper is organized as follows. In Sec. II we discussed the electron-phonon interaction in quantum wires. The Fröhlich couplings are written using the DC model in Sec. II A, the HC model in Sec. II B, and the HZ model in Sec. II C. The electron transport is calculated and analyzed in Sec. III. Section IV concludes the paper.

II. ELECTRON-PHONON INTERACTION IN QUANTUM WIRES

In a cylindrical GaAs (denoted as material 1) quantum wire of radius R and length L ($L \gg R$) embedded in AlAs (denoted as material 2), electrons are confined in GaAs where the potential well develops. Under the infinitely deep well approximation, electron wave functions can be written as

$$\psi_{lj,k}(\mathbf{r}) = \frac{e^{ikz}}{\sqrt{L}} C_j^l J_l\left(x_j^l \frac{r}{R}\right) e^{il\phi}; \quad \begin{cases} l = \ldots, -1, 0, 1, \ldots \\ j = 1, 2, 3, \ldots \end{cases} \tag{1}$$

with the corresponding energies

$$\varepsilon_j^l(k) = \frac{k^2}{2m^*} + \frac{(x_j^l)^2}{2m^* R^2}. \tag{2}$$

Here, $\mathbf{r} = (r, \phi, z)$ are cylindrical coordinates for the system and k denotes the axial wave-vector component. $C_j^l = 1/(\sqrt{\pi} y_j^l R)$ is the normalization factor, x_j^l is the jth zero of the lth order Bessel function, i.e., $J_l(x_j^l) = 0$ and $y_j^l = J_{l+1}(x_j^l)$; m^* is the effective mass of electron.

In Secs. II A–II C, we derive the Fröhlich interaction Hamiltonian in GaAs/AlAs quantum wires within DC, HC, and HZ models.[38] Hamiltonians corresponding to other electron-phonon couplings, such as deformation potential scattering with longitudinal optic and acoustic phonons and piezoelectric interaction with acoustic phonons, are treated with the bulk phonon approximation.[23,37]

A. Dielectric continuum (DC) model

In discussing optic-phonon modes under the dielectric continuum model, a GaAs/AlAs quantum wire can be considered as a single wire of dielectric function $\kappa_1(\omega)$

embedded in material 2 of dielectric function $\kappa_2(\omega)$ and each dielectric function has the form of bulk materials

$$\kappa_i(\omega) = \kappa_{i\infty}\frac{(\omega^2-\omega_{\mathrm{LO}i}^2)}{(\omega^2-\omega_{\mathrm{TO}i}^2)} \tag{3}$$

where ω is the lattice vibration (optic phonon) frequency, $\kappa_{i\infty}$ is the high frequency dielectric constant, and $\omega_{\mathrm{LO}i}$ and $\omega_{\mathrm{TO}i}$ are the longitudinal (LO) and transverse (TO) bulk optic-phonon frequency in material i ($i=1,2$). The electric potentials associated with lattice optic vibrations, $\varphi(\mathbf{r})$, satisfy the equation

$$\kappa_i(\omega)\nabla^2\varphi = 0 \tag{4}$$

with the boundary condition that the potential φ and the normal component of electric displacement $\kappa_i(\omega)d\varphi/dr$ are continuous at the GaAs/AlAs interface.

A confined GaAs LO mode with frequency $\omega=\omega_{\mathrm{LO1}}$ [corresponding to $\kappa_1(\omega)=0$ and $\varphi(\mathbf{r})|_{r>R}=0$ in Eq. (4)] is characterized by an axial wave-vector component q, an angular momentum quantum number m, and an integer quantum number n to distinguish phonon modes of the same q and m, with the potential

$$\varphi(\mathbf{r}) = \begin{cases} CJ_m(q_{m,n}r)e^{im\phi}e^{iqz}\,; & r\geq R \\ 0\,; & r\leq R \end{cases};$$

$$\begin{cases} m=\ldots,-1,0,1,\ldots \\ n=1,2,3,\ldots. \end{cases} \tag{5}$$

Here, $q_{m,n}=x_n^m/R$ is the transverse component of the wave vector and the normalization coefficient C is determined by employing the relation between the potential φ and the reduced ionic displacement $\mathbf{w}$ of a confined LO phonon mode,

$$\nabla\varphi = \omega_{\mathrm{LO}i}\epsilon_0^{-1/2}(\kappa_{i\infty}^{-1}-\kappa_{is}^{-1})^{1/2}\mathbf{w}, \tag{6}$$

where κ_{is} is the static dielectric constant of material i ($i=1,2$).

According to the lattice dynamic theory, the normalized $\mathbf{w}$ is treated as the displacement basis in a harmonic oscillation. The total potential of all phonon modes inside the wire can be expressed as

$$\varphi^{\mathrm{DC}}(\mathbf{r}) = \sum_{q,m,n}\alpha\left(\frac{\omega_{\mathrm{LO1}}}{L}\right)^{1/2}V_{m,n}^{\mathrm{DC}}(r)e^{im\phi} \times e^{iqz}[A_{mn}(q)+A_{mn}^{\dagger}(-q)] \tag{7}$$

with

$$V_{m,n}^{\mathrm{DC}}(r) = \mathcal{C}_{m,n}^{\mathrm{DC}}J_m(q_{m,n}r);\quad \begin{cases} m=\ldots,-1,0,1,\ldots \\ n=1,2,3,\ldots \end{cases} \tag{8}$$

and the normalization constant

$$\mathcal{C}_{m,n}^{\mathrm{DC}} = \frac{1}{\sqrt{\pi}Ry_n^m}\left(\frac{1}{q^2+q_{m,n}^2}\right)^{1/2}. \tag{9}$$

In Eq. (7), $A_{mn}(q)$ [$A_{mn}^{\dagger}(q)$] stands for the annihilation (creation) operator of the confined phonon (q,n,m) and the constant

$$\alpha = \left(\frac{\hbar}{2\epsilon_0}\right)^{1/2}\left(\frac{1}{\kappa_{1\infty}}-\frac{1}{\kappa_{1s}}\right)^{1/2}. \tag{10}$$

The Fröhlich coupling between electrons and confined LO phonons in the DC model is:

$$\begin{aligned} H^{\mathrm{C}} &= -e\sum_{l,l',j,j'}\int d\mathbf{r}\;\psi_{lj}^{*}(\mathbf{r})\varphi^{\mathrm{DC}}(\mathbf{r})\psi_{l'j'}(\mathbf{r}) \\ &= \sum_{l,l',j,j'}\sum_{n,k,q}M_{\mathrm{Fr}}^{\mathrm{DC}}(l,l',j,j',q,n)C_{l,j,k}^{\dagger} \\ &\quad\times C_{l',j',k-q}[A_{l-l',n}(q)+A_{l-l',n}^{\dagger}(-q)]. \end{aligned} \tag{11}$$

Here, $C_{l,j,k}$ ($C_{l,j,k}^{\dagger}$) is the electron annihilation (creation) operator of wave vector k in subband $\{_j^l\}$,

$$M_{\mathrm{Fr}}^{\mathrm{DC}}(l,l',j,j',q,n) = -e\alpha\left(\frac{\omega_{\mathrm{LO1}}}{L}\right)^{1/2} \times\mathcal{C}_{l-l',n}^{\mathrm{DC}}F_{l,l',j,j'}^{\mathrm{C}}(x_n^{l-l'}) \tag{12}$$

is the coupling matrix element and

$$F_{l,l',j,j'}^{\mathrm{C}}(\eta) = 2\int_0^1\xi d\xi\frac{1}{y_j^l y_{j'}^{l'}}J_l(x_j^l\xi)J_{l-l'}(\eta\xi)J_{l'}(x_{j'}^{l'}\xi) \tag{13}$$

is the form factor.[23]

The surface phonons of cylindrical quantum wires in the DC model [corresponding to the conditions $\kappa_i(\omega)\neq 0$ and $\nabla^2\varphi=0$ ($i=1,2$) in Eq. (4)] have been studied previously in Ref. 17. For a mode with axial wave vector q, the potentials $\varphi_s(\mathbf{r})$ in material 1 ($r\leq R$) and 2 ($r\geq R$) are expressed as mth order Bessel functions of imaginary argument I_m and K_m, respectively. The surface phonons play roles in ultrafine GaAs/AlAs quantum wires, where electrons occupy only the ground subband $\{_1^0\}$ and the intersubband transitions can be neglected. Thus it is sufficient to consider the lowest surface phonon mode and

$$\varphi_s(\mathbf{r}) = \begin{cases} C_0K_0(qR)I_0(qr)e^{iqz}; & r\leq R \\ C_0I_0(qR)K_0(qr)e^{iqz}; & r\geq R. \end{cases} \tag{14}$$

The total potential associated with surface optic phonons is obtained, following the normalization method given in Refs. 8 and 16, to be

$$\varphi_s(\mathbf{r}) = \sum_{q,s}\left(\frac{\hbar}{2\epsilon_0\omega_s L}\right)^{1/2}\frac{1}{\sqrt{\pi}qR}\frac{I_0(qr)}{I_0(qR)} \times\mathcal{C}_s(q,\omega_s)[a_s(q)+a_s^{\dagger}(-q)], \tag{15}$$

where $a_s(q)$ [$a_s^{\dagger}(q)$] stands for the annihilation (creation) operator of surface phonons and $\mathcal{C}_s(q,\omega_s)$ is the normalization constant,

$$\mathcal{C}_s^{-2}(q,\omega_s) = \kappa_{1s}\frac{(\omega_{\mathrm{LO1}}^2-\omega_{\mathrm{TO1}}^2)}{(\omega_s^2-\omega_{\mathrm{TO1}}^2)^2}\left[1-\frac{I_2(qR)}{I_0(qR)}\right] +\kappa_{2s}\frac{(\omega_{\mathrm{LO2}}^2-\omega_{\mathrm{TO2}}^2)}{(\omega_s^2-\omega_{\mathrm{TO2}}^2)^2}\left[\frac{K_2(qR)}{K_0(qR)}-1\right]. \tag{16}$$

The surface phonon frequency ω_s is determined by the dispersion relation[17]

$$\kappa_{2\infty}\frac{(\omega_s^2-\omega_{\mathrm{LO2}}^2)K_1(qR)}{(\omega_s^2-\omega_{\mathrm{TO2}}^2)K_0(qR)}+\kappa_{1\infty}\frac{(\omega_s^2-\omega_{\mathrm{LO1}}^2)I_1(qR)}{(\omega_s^2-\omega_{\mathrm{TO1}}^2)I_0(qR)}=0. \tag{17}$$

The sum of s in Eq. (15) is over the two surface branches ω_s^- and ω_s^+, which locate in ranges $\omega_{\mathrm{TO1}}\le\omega_s^-\le\omega_{\mathrm{LO1}}$ (GaAs surface phonons) and $\omega_{\mathrm{TO2}}\le\omega_s^+\le\omega_{\mathrm{LO2}}$ (AlAs surface phonons), respectively. The electron–surface-phonon coupling is given by

$$H^{\mathrm{S}}=\sum_{l,j,j'}\sum_{k,q,s}M^{\mathrm{S}}_{\mathrm{Fr}}(l,l,j,j',q,s)C^{\dagger}_{l,j,k}\times C_{l,j',k-q}[a_s(q)+a_s^{\dagger}(-q)] \tag{18}$$

with the electron-phonon interaction matrix element

$$M^{\mathrm{S}}_{\mathrm{Fr}}(l,l,j,j',q,s)=\frac{-e}{\sqrt{\pi}R}\left(\frac{\hbar}{2\epsilon_0\omega_s L}\right)^{1/2}\times\mathcal{C}_s(q,\omega_s)\frac{1}{q}F^{\mathrm{S}}_{l,l,j,j'}(qR) \tag{19}$$

and the form factor of the surface phonons

$$F^{\mathrm{S}}_{l,l,j,j'}(\eta)=\frac{2}{I_0(\eta)}\int_0^1\xi d\xi\frac{1}{y_j^l y_{j'}^l}J_l(x_j^l\xi)I_0(\eta\xi)J_l(x_{j'}^l\xi). \tag{20}$$

Figure 1 plots form factors $F^{\mathrm{S}}_{l,l,j,j'}(\eta)$ for electron intrasubband scatterings in the ground subband $\{^0_1\}$ and intersubband transitions between subbands $\{^0_1\}$ and $\{^0_2\}$ due to the first surface-phonon mode. Similar to the form factors of bulklike phonon modes $F^{C}_{l,l',j,j'}(\eta)$[23], $F^{\mathrm{S}}_{l,l,j,j'}(\eta)$ approaches unit for intrasubband scatterings and

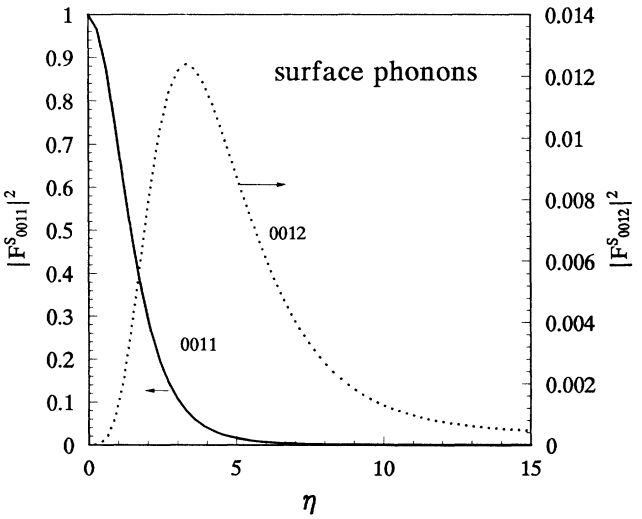

FIG. 1. Illustration of form factors due to surface phonons $F^{s}_{ll'jj'}(\eta)$ [Eq. (20)], where the solid curve corresponds to intrasubband scatterings in the ground subband $\{^0_1\}$ and the dotted curve corresponds to intersubband transitions between subbands $\{^0_1\}$ and $\{^0_2\}$.

vanishes for intersubband transitions at $\eta=0$.

In Ref. 35, Enderlein derived the macroscopic optic-phonon modes in a cylindrical wire including the dispersion of confined phonons by solving the general Born-Huang equation with the Hermiticity condition for the dynamical operator. The same phonon modes as described above [Eqs. (5) and (14)] are obtained. Since the dispersion of confined LO phonons is negligible in the study of electron transport, the dispersionless DC optic-phonon model is expected to give the same results as the macroscopic model developed by Enderlein does.

B. Hydrodynamic continuum (HC) model

In the HC model, the optic-phonon modes are obtained by solving the general Born-Huang equation under the hydrodynamic boundary condition for optic displacement, which requires the continuity of the normal component of the velocity and the continuity of the pressure, as suggested by Babiker.[11,25] Since the spectra of GaAs and AlAs do not overlap in frequency, surface phonons do not exist in the hydrodynamic continuum (HC) model,[5,18,25] and only the confined phonons need be considered.

Since Ridley treated the LO phonons in quantum wells,[12] we employ a simple dispersive HC model to describe optic-phonon modes in GaAs/AlAs quantum wires. In this model, the phonon displacement vanishes and the corresponding potential reaches its maximum at the interface. This boundary condition is approximate,[36] but it is accurate enough to obtain the phonon modes for transport calculation. The reduced ionic displacement field $\mathbf{w}=(w_r,w_\phi,w_z)$ of a phonon mode in GaAs satisfies the Helmholtz equation

$$(\nabla^2+q^2)\mathbf{w}=0 \tag{21}$$

with the boundary condition

$$w_r|_{r=R}=0. \tag{22}$$

The frequency takes the form

$$\omega^2=\omega_{\mathrm{LO1}}^2-\beta^2(q^2+q_{\|}^2), \tag{23}$$

where β is the velocity parameter of GaAs, and $q_{\|}$ is the transverse wave vector of the phonon mode.

Each confined phonon is characterized by three parameters, q,m, and n, as denoted in the DC model, and the total optic-phonon potential can be written as

$$\varphi^{\mathrm{HC}}=\sum_{m,n,q}\alpha\left(\frac{\omega_{\mathrm{LO1}}^2}{\omega_{m,n}L}\right)^{1/2}V^{\mathrm{HC}}_{m,n}e^{im\phi}e^{iqz}\times[A_{mn}(q)+A^{\dagger}_{mn}(-q)] \tag{24}$$

with

$$V^{\mathrm{HC}}_{m,n}=\mathcal{C}^{\mathrm{HC}}_{m,n}J_m(q_{m,n}r);\quad\begin{cases}m=\ldots,-1,0,1,\ldots\\ n=1,2,3,\ldots.\end{cases} \tag{25}$$

Here, the normalization constant

$$C^{\mathrm{HC}}_{m,n} = \frac{1}{\sqrt{j'^2_{m,n} - m^2}} \frac{1}{J_m(j'_{m,n})} \frac{q_{m,n}}{(q^2 + q^2_{m,n})^{1/2}}, \quad (26)$$

and the transverse wave-vector component $q_{\|} = q_{m,n} = j'_{m,n}/R$, $j'_{m,n}$ is the nth zero of mth order Bessel function derivative, i.e., $J'_m(j'_{m,n}) = 0$, $\omega_{m,n}$ is the phonon frequency determined by the dispersion relation [Eq. (23)]. The corresponding electron-phonon Hamiltonian has the same form as in the DC model [Eq. (11)] but with a different matrix element:

$$M^{\mathrm{HC}}_{\mathrm{Fr}}(l,l',j,j',q,n) = -e\alpha \left(\frac{\omega^2_{\mathrm{LO1}}}{\omega_{m,n}L}\right)^{1/2} \times C^{\mathrm{HC}}_{l-l',n} F^{\mathrm{C}}_{l,l',j,j'}(j'_{l-l',n}). \quad (27)$$

C. Huang-Zhu (HZ) model

According to the results of the lattice dynamic theory of Huang and Zhu,[6] both the normal optic displacement and the potential should vanish at the interface in quantum wells and rectangular quantum wires.[6] By assuming that the same boundary conditions are satisfied in cylindrical quantum wires, we propose here the confined optic-phonon modes in the HZ model. Numerical calculation shows that the phonon frequency dispersion has little effect on the electron transport investigated in this paper; we thus consider a dispersionless model.

Taking advantage of clues from a simple microscopic model[6] calculation in rectangular quantum wires, we can compose the potential of a confined phonon mode in the cylindrical quantum wire from a Bessel function plus a simple term. This term is a constant for a reverse symmetric mode with maximum potential at the center of the wire, a linear one for a reverse antisymmetric mode, and a square term for a reverse symmetric mode with vanishing potential at the center of the quantum wire. The Fröhlich potential of confined optic phonons in the HZ model can be expressed as

$$\varphi^{\mathrm{HZ}}(\mathbf{r}) = \sum_{m,n,q} \alpha \left(\frac{\omega_{\mathrm{LO1}}}{L}\right)^{1/2} V^{\mathrm{HZ}}_{m,n} e^{im\phi} \times e^{iqz}[A_{m,n}(q) + A^{\dagger}_{m,n}(-q)], \quad (28)$$

with

$$V^{\mathrm{HZ}}_{m,n} = \frac{1}{\sqrt{\pi}} C^{\mathrm{HZ}}_{m,n} \Phi_{m,n}(r); \quad \begin{cases} m = \ldots, -1, 0, 1, \ldots \\ n = 1, 2, 3, \ldots . \end{cases} \quad (29)$$

Here,

$$\Phi_{m,n}(r) = \begin{cases} J_0(x^1_n \frac{r}{R}) - J_0(x^1_n); & \text{for } m = 0 \\ J_m(h^m_n \frac{r}{R}) - J_m(h^m_n)\frac{r}{R}; & \text{for } |m| = 2s+1, \quad s = 0, 1, 2, \ldots \\ J_m(g^m_n \frac{r}{R}) - J_m(g^m_n)(\frac{r}{R})^2; & \text{for } |m| = 2s, \quad s = 1, 2, 3, \ldots \end{cases} \quad (30)$$

with zeros g^m_n and h^m_n fulfilling equations

$$h^m_n J'_m(h^m_n) - J_m(h^m_n) = 0 \quad (31)$$

and

$$g^m_n J'_m(g^m_n) - 2J_m(g^m_n) = 0, \quad (32)$$

respectively. The series of h^m_n and g^m_n are determined by solving Eqs. (31) and (32) in the ranges

$$x^{m+1}_n \le h^m_n,\ g^m_n < j'_{m,n+1},$$

and

$$\begin{cases} h^1_n = x^2_n; \\ h^3_1 = 7.869; \quad h^3_2 = 11.25; \quad \ldots; \\ h^5_1 = 10.40; \quad h^5_2 = 13.91; \quad \ldots; \end{cases} \quad \begin{cases} g^2_n = x^3_n; \\ g^4_1 = 9.017; \quad g^4_2 = 12.51; \quad \ldots; \\ g^6_1 = 11.50; \quad g^6_2 = 15.11; \quad \ldots . \end{cases} \quad (33)$$

Note that phonon modes corresponding to solutions of Eqs. (31) or (32) in ranges of $0 < h^m_0, g^m_0 < j'_{m,1}$ do not exist actually because they are identical to modes of h^m_1 or g^m_1. $C^{\mathrm{HZ}}_{m,n}$ is the normalization coefficient, for $m = 0$,

$$(C^{\mathrm{HZ}}_{0,n})^{-2} = [2q^2R^2 + (x^1_n)^2]\, J^2_0(x^1_n), \quad (34)$$

for $|m| = 2s+1$; $s = 0, 1, 2, \ldots$,

$$(C^{\mathrm{HZ}}_{m,n})^{-2} = (h^m_n)^2 J^2_m(h^m_x) - \frac{16s(s+1)}{h^m_n} J_{|m|}(h^m_n)\Gamma_s(h^m_n) + (qR)^2 \left\{ \left[\frac{3}{2} - \frac{4s(s+1)}{(h^m_n)^2}\right] J^2_m(h^m_n) - \frac{16s(s+1)}{(h^m_n)^3} J_{|m|}(h^m_n)\Gamma_s(h^m_n) \right\} \quad (35)$$

and for $|m| = 2s$; $s = 1, 2, 3, \cdots$,

$$(\mathcal{C}^{\rm HZ}_{m,n})^{-2} = J^2_m(g^m_n)\left[-2s^2+2-\frac{32(s-1)^2(s+1)}{(g^m_n)^2}+(g^m_n)^2\right]-\frac{32s(s^2-1)}{(g^m_n)^2}J_{|m|}(g^m_n)\Gamma_s(g^m_n)$$
$$+(qR)^2\left\{\left[\frac{4}{3}-\frac{4(s^2-1)}{(g^m_n)^2}-\frac{32s(s-1)^2(s+1)}{(g^m_n)^4}\right]J^2_m(g^m_n)-\frac{32s(s^2-1)}{(g^m_n)^4}J_{|m|}(g^m_n)\Gamma_s(g^m_n)\right\}, \quad (36)$$

where

$$\Gamma_0(\xi) = 1 - J_0(\xi)$$
$$\Gamma_s(\xi) = 1 - 2\sum_{k=1}^{s} J_{2k}(\xi) - J_0(\xi); \quad \text{for } s \geq 1.$$

In the case of $q = 0$, values of the series of $\mathcal{C}^{\rm HZ}_{m,n}$ are

$$\begin{cases} \mathcal{C}^{\rm HZ}_{01} = 0.6479; & \mathcal{C}^{\rm HZ}_{02} = 0.4750; & \mathcal{C}^{\rm HZ}_{03} = 0.3937; \ldots \\ \mathcal{C}^{\rm HZ}_{11} = 0.5733; & \mathcal{C}^{\rm HZ}_{12} = 0.4378; & \mathcal{C}^{\rm HZ}_{13} = 0.3702; \ldots \\ \mathcal{C}^{\rm HZ}_{21} = 0.5533; & \mathcal{C}^{\rm HZ}_{22} = 0.4197; & \mathcal{C}^{\rm HZ}_{23} = 0.3562; \ldots . \end{cases} \quad (37)$$

Thus the electron-phonon coupling matrix element reads

$$M^{\rm HZ}_{\rm Fr}(l,l',j,j',q,n) = -e\alpha\left(\frac{\omega_{\rm LO1}}{\pi L}\right)^{1/2} \times \mathcal{C}^{\rm HZ}_{m,n} F^{\rm HZ}_{l,l',j,j'}(q_{l-l',n}R), \quad (38)$$

where the transverse wave vector

$$q_{m,n} = \begin{cases} x^1_n/R; & \text{for } m = 0 \\ h^m_n/R; & \text{for } |m| = 2s+1; \quad s = 0,1,2,\ldots \\ g^m_n/R; & \text{for } |m| = 2s; \quad s = 1,2,3,\ldots \end{cases} \quad (39)$$

and the form factor

$$F^{\rm HZ}_{l,l',j,j'}(\eta) = \int_0^1 \xi d\xi \frac{2}{y^l_j y^{l'}_{j'}} J_l(x^l_j\xi) \times \Phi_{l-l',n}(\eta\xi) J_{l'}(x^{l'}_{j'}\xi). \quad (40)$$

The form factors for intrasubband coupling in the ground subband $\{^0_1\}$ and intersubband transitions between subbands $\{^0_1\}$ and $\{^1_1\}$ are shown in Fig. 2.

It is worthy of note that the phonon modes of the HZ model are *ad hoc* as pointed out by Nash[14] and Constantinou.[28] However, they are convenient and accurate enough to estimate the electron transport in this paper. In fact, for wave vectors of interest in electron-phonon scattering, they are almost the same as those obtained from the recently developed hybridization theory.[28,39]

The surface phonon modes in the HZ model are the same as those in the DC model[6] and the corresponding Hamiltonian has been given in Eq. (18).

The factor $V_{0,1}(r)$ in the Fröhlich potential of the first confined phonon mode in Eqs. (8), (25), and (29) is illustrated in Fig. 3 as a function of the quantum wire radius for different models. The curve (dotted) of the HZ model is close to that of the DC model while the potential of the HC model (dashed line) vanishes inside the wire and has a much smaller value than those in other two models at the center of the quantum wire. This results in a much lower scattering rate in the HC model, as shown in the following section.

The following parameter values were used in the calculation of this paper: for GaAs, $\omega_{\rm LO1} = 36.2$ meV, $\omega_{\rm TO1} = 33.3$ meV, and $\kappa_{1\infty} = 10.9$; for AlAs, $\omega_{\rm LO2} = 50.1$ meV, $\omega_{\rm TO2} = 44.8$ meV, and $\kappa_{2\infty} = 8.16$; In the HC model, the velocity parameter for GaAs is $\beta = 4.73 \times 10^3$ m/s.

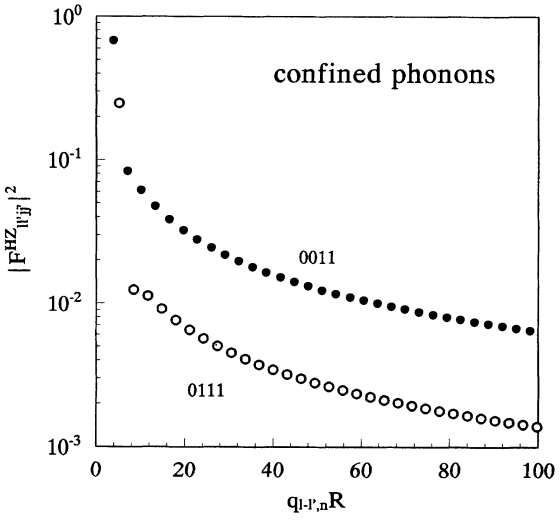

FIG. 2. Form factors for confined phonons in the HZ model $F^{\rm HZ}_{ll'jj'}(q_{l-l',n}R)$ [Eq. (40)] at different zeros of Φ. Values of intrasubband couplings in the ground subband $\{^0_1\}$ (dots) and intersubband transitions between subbands $\{^0_1\}$ and $\{^1_1\}$ (circles) are shown.

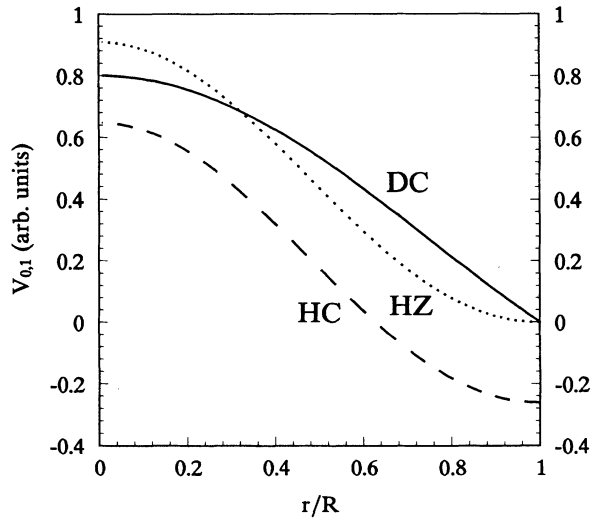

FIG. 3. The Fröhlich potentials of the lowest confined phonon mode in the dielectric continuum (solid line), hydrodynamic continuum (dashed line), and Huang-Zhu models (dotted line) are compared.

III. ELECTRON TRANSPORT: RESULTS AND DISCUSSIONS

Under the influence of a longitudinal electric field, electrons drift along the quantum wire. Such a transport state is described in the balance equation transport theory[23,37] by two parameters, the electron drift velocity v_d and the electron temperature T_e, and they are determined by the force- and energy-balance equations of the system in steady state,

$$eE + f(v_d) = 0, \tag{41}$$

$$v_d f(v_d) + w(v_d) = 0. \tag{42}$$

We assume that elastic scatterings are negligible such that the frictional force $f(v_d)$ and energy loss rate $w(v_d)$ per electron are due to phonon scatterings,

$$f(v_d) = \frac{2}{n_3\pi R^2}\sum_{\substack{l,l',j,j'\\ \mathbf{q},\lambda}} |M_{ll'jj'}(\mathbf{q},\lambda)|^2 q\Pi_2(l,l',j,j',q,\Omega_{\mathbf{q}\lambda}+qv_d)\{n(\Omega_{\mathbf{q}\lambda}/T)-n[(\Omega_{\mathbf{q}\lambda}+qv_d)/T_e]\}$$
$$+\frac{2}{n_3\pi R^2}\sum_{\substack{l,l',j,j'\\ q,\Lambda}} |M_{\mathrm{Fr}}(l,l',j,j',q,\Lambda)|^2 q\Pi_2(l,l',j,j',q,\Omega_{q\Lambda}+qv_d)\{n(\Omega_{q\Lambda}/T)-n[(\Omega_{q\Lambda}+qv_d)/T_e]\} \tag{43}$$

and

$$w(v_d) = \frac{2}{\pi n_3 R^2}\sum_{\substack{l,l',j,j'\\ \mathbf{q},\lambda}} |M_{ll'jj'}(\mathbf{q},\lambda)|^2 \Omega_{\mathbf{q}\lambda}\Pi_2(l,l',j,j',q,\Omega_{\mathbf{q}\lambda}+qv_d)\{n(\Omega_{\mathbf{q}\lambda}/T)-n[(\Omega_{\mathbf{q}\lambda}+qv_d)/T_e]\}$$
$$+\frac{2}{\pi n_3 R^2}\sum_{\substack{l,l',j,j'\\ q,\Lambda}} |M_{\mathrm{Fr}}(l,l',j,j',q,\Lambda)|^2 \Omega_{q\Lambda}\Pi_2(l,l',j,j',q,\Omega_{q\Lambda}+qv_d)\{n(\Omega_{q\Lambda}/T)-n[(\Omega_{q\Lambda}+qv_d)/T_e]\}. \tag{44}$$

Here, $M_{\mathrm{Fr}}(l,l',j,j',q,\Lambda)$ stands for the matrix element of Fröhlich interaction between electrons and GaAs LO confined phonons ($\Lambda = n$) or surface phonons ($\Lambda = s$ in DC and HZ models), $\Omega_{q,\Lambda}$ is the corresponding phonon frequency, and $M_{ll'jj'}(\mathbf{q},\lambda)$ represents the matrix element of the other electron-phonon coupling mechanisms,[37] n_3 is the electron bulk density corresponding to a wire density $n_l = \pi R^2 n_3$, Π_2 is the imaginary part of the electron density-density correlation function in the quantum wire,[23,37] and $n(x) \equiv [\exp(x)-1]^{-1}$ is the Bose function. The electron inverse mobility $1/\mu = E/v_d = -f(v_d)/n_l e v_d$ comprises the contribution from electron–LO-phonon (Fröhlich) interaction μ_p^{-1} and that from other electron-phonon couplings μ_0^{-1}. μ_p^{-1} comes from confined phonons (μ_c^{-1}) and (in DC and HZ models) from the surface phonon (μ_s^{-1}). Thus, $\mu^{-1} = \mu_0^{-1} + \mu_p^{-1} = \mu_0^{-1} + \mu_c^{-1} + \mu_s^{-1}$.

First, we calculate electron linear mobilities in cylindrical GaAs/AlAs quantum wires with various lateral extensions but the same bulk carrier density at temperature $T = 300$ K. In Fig. 4, inverse linear mobilities μ_p^{-1} obtained using different phonon models are plotted as functions of the wire diameter d. The result shows that linear mobilities from DC and HZ models and from the bulk phonon approximation (BK) have almost the same values over the whole lateral confinement range, while the HC model gives a much higher mobility in small quantum wires.

Confined-phonon-induced inverse linear mobilities μ_c^{-1} and surface-phonon-induced inverse linear mobility μ_s^{-1} are plotted as functions of the wire diameter d respectively in Fig. 5 in the same condition as in Fig. 4. At the large wire diameter, the surface phonons are negligible and the confined phonons account for all the optic-phonon effects on the electron transport. When d shrinks, the surface phonon contribution, which begins to influence the electron transport at a wire diameter about $d = 20$ nm, increases rapidly ($\sim d^{-2}$) and exceeds that of the confined phonons when $d < 5$ nm. In extremely small wire ($d < 3$ nm), the surface-phonon-induced inverse mobility (μ_s^{-1}) has the same value as the inverse mobility

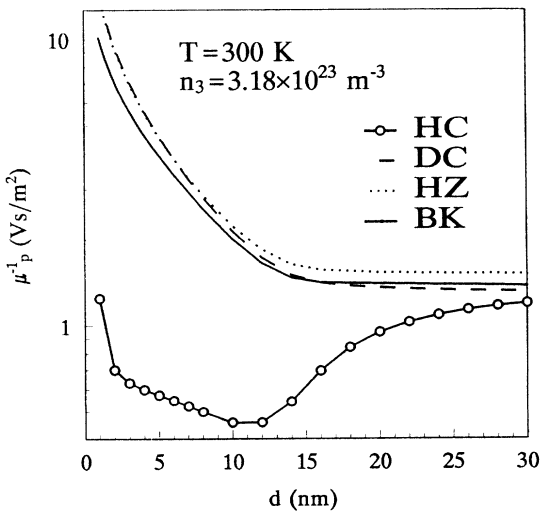

FIG. 4. Wire diameters d dependence of the LO phonon Fröhlich-interaction-induced linear inverse mobility of electrons in a cylindrical GaAs/AlAs quantum wire in the hydrodynamic continuum model (circle line), the dielectric continuum model (dashed line), the Huang-Zhu (dotted line) model, and the bulk-phonon approximation (solid line) at room temperature $T = 300$ K.

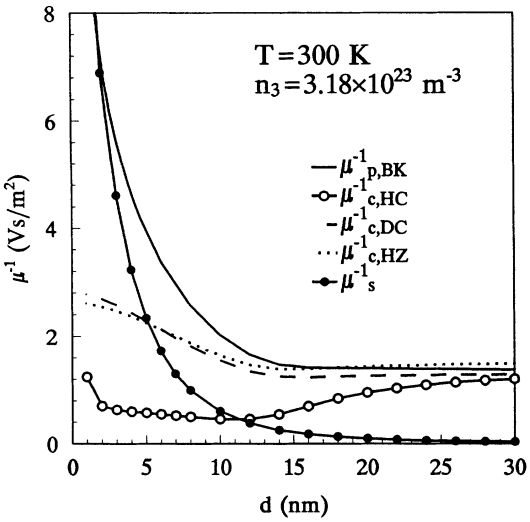

FIG. 5. The inverse mobilities due to confined and surface phonons are plotted respectively as functions of quantum wire diameter in the same condition as Fig. 4.

calculated from the bulk phonon approximation ($\mu^{-1}_{p,\mathrm{BK}}$) while the contribution of confined phonons becomes very small. It is worth noting that the inverse mobility from the HC model ($\mu^{-1}_{c,\mathrm{HC}}$) is even much smaller than the values caused by confined phonons in DC ($\mu^{-1}_{c,\mathrm{DC}}$) and HZ ($\mu^{-1}_{c,\mathrm{HZ}}$) models. For example, $\mu^{-1}_{c,\mathrm{HC}} \sim 0.25\mu^{-1}_{c,\mathrm{DC}}$ in quantum wires of $d = 5$ nm. This stems from the much lower potential of the first phonon mode in the HC model as illustrated in Fig. 3. Because electrons stay in the ground subband and only the first confined optic-phonon mode contributes to the Fröhlich interaction in small quantum wires ($d < 10$ nm), the above mobility difference can be roughly estimated from a direct comparison between matrix elements in different models.

The squares of Fröhlich coupling matrix elements between confined phonons and electrons in the electron ground subband are

$$|M^{\mathrm{DC}}_{\mathrm{Fr}}(0,0,1,1,q,1)|^2 = \frac{1}{(y^0_1)^2[(qR)^2+(x^0_1)^2]}|F^{\mathrm{C}}_{0,0,1,1}(x^0_1)|^2\chi,$$

$$|M^{\mathrm{HC}}_{\mathrm{Fr}}(0,0,1,1,q,1)|^2 = \frac{1}{J^2_0(j'_{0,2})[(qR)^2+(j'_{0,2})^2]}|F^{\mathrm{C}}_{0,0,1,1}(j'_{0,2})|^2\chi,$$

$$|M^{\mathrm{HZ}}_{\mathrm{Fr}}(0,0,1,1,q,1)|^2 = \frac{1}{J^2_0(x^1_1)[(qR)^2+(x^1_1)^2]}|F^{\mathrm{HZ}}_{0,0,1,1}(x^1_1)|^2\chi,$$

where χ has the same value for different models and the optimum wave vector for phonons to contribute to the electron transport is about (from the numerical calculation) $qR = 1$ for $R = 2.5$ nm. Substituting the values of constants $x^0_1 = 2.4$, $y^0_1 = 0.52$, $j'_{0,2} = x^1_1 = 3.83$, $J_0(j'_{0,2}) = -0.4$ and the values of form factors[23] $|F^{\mathrm{C}}_{0,0,1,1}(x^0_1)|^2 = 0.525$, $|F^{\mathrm{C}}_{0,0,1,1}(j'_{0,2})|^2 = 0.17$, $|F^{\mathrm{HZ}}_{0,0,1,1}(x^1_1)|^2 = 0.68$ into above equations, we have $|M^{\mathrm{DC}}_{\mathrm{Fr}}|^2 = 0.28\chi$, $|M^{\mathrm{HC}}_{\mathrm{Fr}}|^2 = 0.068\chi$, and $|M^{\mathrm{HZ}}_{\mathrm{Fr}}|^2 = 0.27\chi$. The scattering rate from HC model is about one-fourth of those from DC and HZ models.

We have also studied the high-field mobility of electrons at different lattice temperatures. In Fig. 6(a), LO phonon induced inverse mobility μ_p^{-1} is plotted as functions of wire diameter d in the presence of an electron drift velocity $v_d = 7.94 \times 10^4$ m/s at lattice temperature $T = 10$ K for different phonon models. Just as in the linear case, DC and HZ models yield almost the same results as the BK does, while the HC model gives a scat-

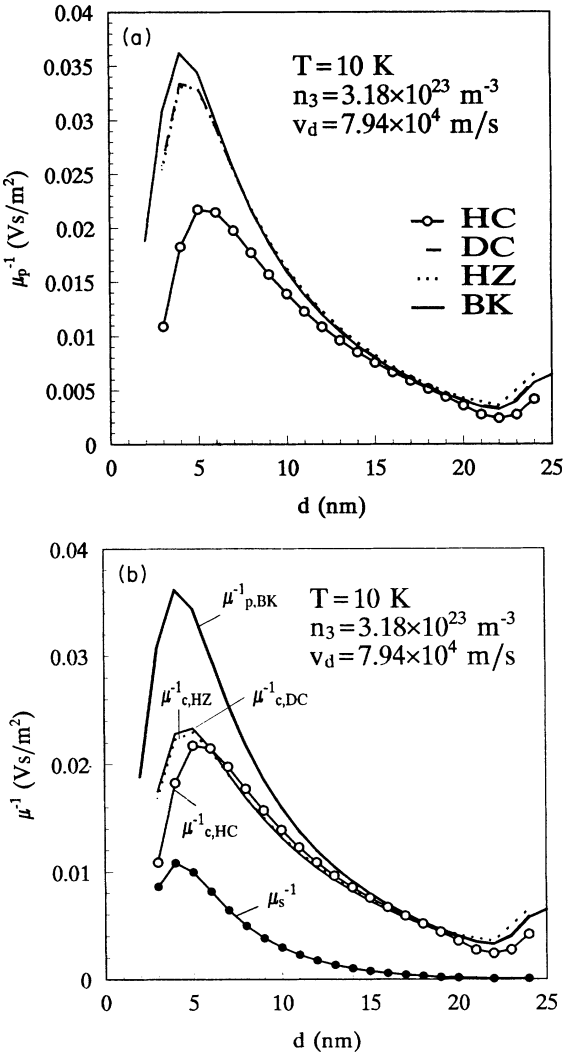

FIG. 6. The wire diameter dependence of high-field inverse mobility due to Fröhlich interaction in different phonon models at lattice temperature $T = 10$ K and electron drift velocity $v_d = 7.94 \times 10^4$ m/s are illustrated in (a) and the inverse mobility is redrawn by separating contributions of confined phonons and surface phonons in (b). Electron subband effects are shown.

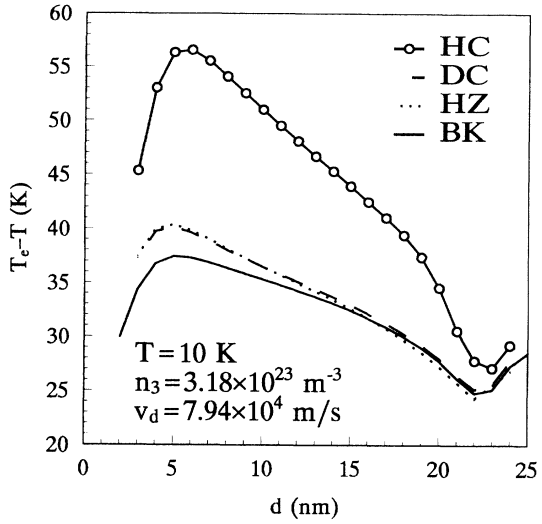

FIG. 7. The electron temperature increment corresponding to the condition of Fig. 6 is graphed versus the wire diameter. The results from different phonon models are compared with that given by the bulk phonon approximation.

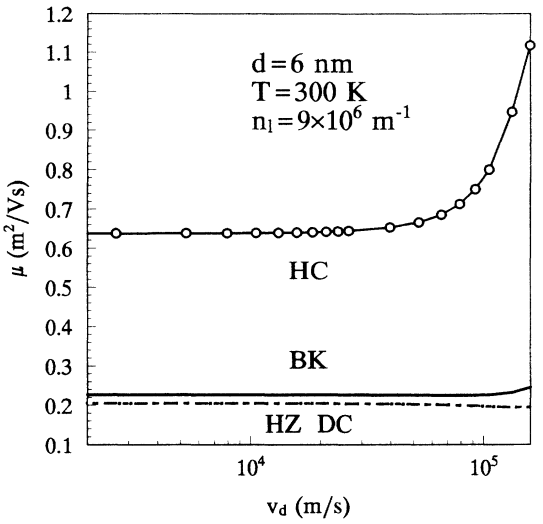

FIG. 8. Electron mobilities μ against the drift velocity v_d in a narrow quantum wire of diameter 6 nm at lattice temperature $T = 300\,\mathrm{K}$ are calculated in different phonon models. Here, HZ and DC models give almost the same curve.

tered result, especially when the Fermi energy is close to the top or bottom of a subband (corresponding to the maximum or minimum of the mobility as a consequence of electron subband effects[23]).

Figure 6(b) distinguishes confined phonon and surface phonon contributions in Fig. 6(a). Different from the linear case, here the confined-phonon-induced mobility in HC model $\mu_{c,\mathrm{HC}}$ is close to those in DC and HZ models because the smaller electron-phonon coupling happens to be compensated by the higher electron temperature required in this model as illustrated in Fig. 7, where the electron temperature increments at drift velocity $v_d = 7.94 \times 10^4\,\mathrm{m/s}$ are plotted as functions of the wire diameter d. The curves belonging to DC and HZ models are just the same and both are close to that of the bulk phonon approximation.

Finally, the drift velocity (and then the electric field) dependence of electron mobility in a quantum wire of diameter $d = 6\,\mathrm{nm}$ at lattice temperature $T = 300\,\mathrm{K}$ is calculated using different optic-phonon models as shown in Fig. 8. The result shows the same conclusion as specified above, i.e., DC and HZ models predict the same electron transport behavior as the bulk-phonon approximation does, but the HC model results in a very different one. This conclusion can be easily generalized to cases in the presence of impurity scatterings.

The above results support the conclusion obtained by Nash:[14] electron-phonon scattering rates should be independent of the basis set used to describe the phonon modes. Because the lattice structure of AlAs is similar to that of GaAs, the influence of AlAs on electron transport through the GaAs/AlAs interface is negligible. The phonon modes of HC model used in this paper, however, may be incomplete since the surface phonon modes, which have been observed experimentally, do not exist in this model.

IV. CONCLUSION

We have calculated the linear and nonlinear electron mobilities in GaAs/AlAs cylindrical quantum wires of various lateral extensions with the help of balance equation transport theory using the dielectric continuum model, hydrodynamic continuum model, and Huang-Zhu model to describe the confined and surface optic-phonon, respectively. The DC model and the HZ model predict the same electron transport properties (linear and nonlinear mobilities and electron temperature) in quantum wires as that obtained using the bulk-phonon approximation, while the HC model gives a scattered result in small quantum wires. Since the HC model is not applicable to the description of surface phonon modes in GaAs/AlAs quantum wires, the phonon modes of this model may be incomplete as pointed out by Nash[14] and should be superseded by the phonon modes of the more realistic continuum model developed recently.[27] We conclude that only bulk optic-phonon description is good enough for the calculation of the electron transport in GaAs/AlAs quantum wires. In DC and HZ models, surface optic phonons begin to contribute to the electron mobility in quantum wire of diameter about 20 nm, and dominate when the wire diameter is less than 5 nm. These conclusions are consistent with the results obtained by Tsuchiya and Ando in GaAs/AlAs superlattices,[15] and confirm the general statement drawn by Nash.[14]

[1]A. K. Sood, J. Menendez, M. Cardona, and K. Ploog, Phys. Rev. Lett. **54**, 2111 (1985).
[2]D. S. Kim, A. Bouchalkha, J. M. Jacob, J. F. Zhou, and J. J. Song, Phys. Rev. Lett. **68**, 1002 (1992).
[3]L. Colombo *et al.*, in *The 21st International Conference on the Physics of Semiconductors*, edited by P. Jiang and H. Z. Zheng (World Scientific, Singapore, 1992), pp. 777—780.
[4]B. K. Ridley, Rep. Prog. Phys. **54**, 169 (1991).
[5]H. Rücker, E. Molinari, and P. Lugli, Phys. Rev. B **44**, 3463 (1991); **45**, 6747 (1992); E. Molinari, C. Bungaro, M. Gulia, P. Lugli, and H. Rücker, Semicond. Sci. Technol. **7**, B67 (1992).
[6]K. Huang and B. Zhu, Phys. Rev. B **38**, 13 377 (1988); **38**, 2183 (1988); B. Zhu, *ibid.* **44**, 1926 (1991).
[7]H. Akera and T. Ando, Phys. Rev. B **40**, 2914 (1989).
[8]N. Mori and T. Ando, Phys. Rev. B **40**, 6175 (1989).
[9]R. Fachs and K. L. Kliewer, Phys. Rev. **140**, A2076 (1965).
[10]M. V. Klein, IEEE J. Quantum Electron. **QE-22**, 1760 (1986).
[11]M. Babiker, J. Phys. C **19**, 683 (1986).
[12]B. K. Ridley, Phys. Rev. B **39**, 5282 (1989).
[13]R. Enderlein, Phys. Rev. B **43**, 14 513 (1991).
[14]K. J. Nash, Phys. Rev. B **46**, 7723 (1992).
[15]T. Tsuchiya and T. Ando, Semicond. Sci. Technol. **7**, B73 (1992).
[16]M. A. Stroscio, Phys. Rev. B **40**, 6428 (1989); M. A. Stroscio, K. W. Kim, M. A. Littlejohn, and H. Chuang, *ibid.* **42**, 1488 (1990); K. W. Kim, M. A. Stroscio, A. Bhatt, R. Mickevicius, and V. V. Mitin, J. Appl. Phys. **70**, 319 (1991).
[17]P. A. Knipp and T. L. Reinecke, Phys. Rev. B **45**, 9091 (1992); **48**, 5700 (1993); R. Ruppin and R. Englman, Rep. Prog. Phys. **33**, 149 (1970).
[18]B. F. Zhu, Phys. Rev. B **46**, 13 619 (1992).
[19]M. Watt, C. M. S. Torres, H. E. G. Arnot, and S. P. Beaumont, Semicond. Sci. Technol. **5**, 285 (1990).
[20]D. G. Hasko, A. Potts, J. R. A. Cleaver, C. G. Smith, and H. Ahmed, J. Vac. Sci. Technol. B **6**, 1849 (1988).
[21]K. Ismail, D. A. Antoniadis, and H. I. Smith, Appl. Phys. Lett. **54**, 1130 (1989).
[22]L. Birotheau *et al.*, Appl. Phys. Lett. **61**, 3023 (1992).
[23]X. F. Wang and X. L. Lei, Phys. Status Solidi B **175**, 433 (1993); X. F. Wang and X. L. Lei, Phys. Rev. B **47**, 16 612 (1993), and reference therein.
[24]V. B. Campos, S. Das Sarma, and M. A. Stroscio, Phys. Rev. B **46**, 3849 (1992); S. Das Sarma, V. B. Campos, M. A. Stroscio, and K. W. Kim, Semicond. Sci. Technol. **7**, B60 (1992).
[25]M. Babiker, Semicond. Sci. Technol. **7**, B52 (1992)
[26]B. K. Ridley and M. Babiker, Phys. Rev. B **43**, 9096 (1991).
[27]B. K. Ridley, Phys. Rev. B **47** 4592 (1993); N. C. Constantinou, O. Al-Dossary and B. K. Ridley, Solid State Commun. **86** 191 (1993).
[28]N. C. Constantinou, in *Phonons in Semiconductor Nanostructures*, edited by J. P. Leburton *et al.* (Kluwer Academic Publishers, Netherlands, 1993), pp. 113–119.
[29]S. Rudin and T. L. Reinecke, Phys. Rev. B **41**, 7713 (1990); **43**, 9298 (1991).
[30]G. Weber, A. M. de Paula, and J. F. Ryan, Semicond. Sci. Technol. **6**, 397 (1991).
[31]J. K. Jain and S. Das Sarma, Phys. Rev. Lett. **62**, 2305 (1989).
[32]H. Gerecke and F. Bechstedt, Semicond. Sci. Technol. **7**, B80 (1992).
[33]M. P. Chamberlain, D. Hoare, R. W. Kelsall, and R. A. Abram, Semicond. Sci. Technol. **7**, B45 (1992); M. P. Chamberlain, M. Babiker and B. K. Ridley, Superlatt. Microstruct. **9**, 227 (1991).
[34]H. León *et al.*, Phys. Status Solidi B **170**, 449 (1992).
[35]R. Enderlein, Phys. Rev. B **47**, 2162 (1993); P. E. Selbmann and R. Enderlein, Superlatt. Microstruct. **12**, 219 (1992).
[36]N. C. Constantinou and B. K. Ridley, Phys. Rev. B **41**, 10 622 (1990); **41**, 10 627 (1990).
[37]X. L. Lei and C. S. Ting, Phys. Rev. B **30**, 4809 (1984); **32**, 1112 (1985); X. L. Lei, J. L. Birman, and C. S. Ting, J. Appl. Phys. **58**, 2270 (1985); X. L. Lei *et al.*, Phys. Rev. B **33**, 4382 (1986); X. L. Lei and N. J. M. Horing, Int. J. Mod. Phys. B **6**, 805 (1992).
[38]The properties of mathematical functions used in the derivation can be found in *Handbook of Mathematical Functions*, edited by M. Abramowitz and I. A. Stegun (Dover, New York, 1972).
[39]X. F. Wang and X. L. Lei (unpublished).